Journal of the Optical Society of Korea, Vol. 5, No. 4, December 2001, pp. 123-130

# Measurement of Absorption Coefficient for Quantum Confined Stark Effect InGaAsP/InP MQW and Refractive Index Change

Ju-Bin Song* and R. Killey

*Department of Electronic and Electrical Engineering, University College of London, Torrington Place, London WC1E 7JE, UK*

(Received June 21, 2001)

In this paper, we report measurement of absorption coefficient for various InGaAsP MQW QCSE device structures. The absorption spectra over a range of QCSE were obtained from measured photocurrent spectra. The refractive index changes with applied electric field were calculated from the absorption spectra.

*OCIS code :* 300.6470.

## I. INTRODUCTION

Various kinds of InGaAsP MQW QCSE devices are to be an important key element for high bit rate optical soliton transmission and dense wavelength division multiplex (DWDM) networks [1]- [4]. There are several reports on QCSE with limited InP based material system and MQW structures [5]- [8].

In this paper, the absorption spectra of the five different active region materials were measured over a range of applied electric fields, the reflectivity spectra of DBRs were measured and compared with the theoretical spectra, and the wafer structure, doping, and contact metals were optimised to obtain good electrical and optical characteristics of the devices. All the wafers were grown by MOVPE and processed at the III-V Semiconductor Facility at the University of Sheffield.

## II. QUANTUM WELL DESIGN

For a QCSE device to be good for soliton generation, transmission, or tuneable FM lasers, it must operate at multi-10 GHz frequencies, with milliwatt peak powers and have as low a loss as possible to avoid the build-up of excess ASE noise associated with the extra amplification required to overcome this loss. Consequently, the important characteristics of a good active region material are (i) a large electro-optic effect and (ii) high saturation intensity and operating frequency. Condition (i) can be satisfied by employing quantum wells in the active material. However, the design of the wells also has an effect on the saturation intensity and frequency. The saturation intensity, $I_S$, is defined as the intensity at which the material absorption change with electric field is half of its value at low intensity, $\Delta\alpha_0$.

$$\Delta\alpha(I) = \frac{\Delta\alpha_0}{1 + (I/I_S)} \tag{1}$$

where $I$ is the optical intensity. The electroabsorption dependency on optical intensity is attributable to two mechanisms [9]. The first is exciton saturation. There is a finite exciton density of states, and as these are filled, the absorption of photons at the exciton energy is reduced. The second effect occurs once the exciton has been created and split apart into a separate electron and hole. These are then removed either by recombination, or, more commonly, by sweep-out due to the applied electric field. If the lifetimes of the two types of carriers are different, a space charge is created in the material which screens the applied field used to achieve the Stark shift.

To maximise the saturation intensity, the active region material must be designed to obtain short sweep-out times of the carriers, to reduce both exciton saturation and the build-up of space charge. Certain design features have been found to accomplish this, including (i) a low bandgap energy difference, $\Delta E_g$, between the well and barrier, (ii) a low well width and (iii) operation with a large applied electric field. In some cases there must be a trade-off in the design to achieve a reasonably high saturation intensity and a good electro-optic effect [9]. For example, reducing $\Delta E_g$ increases the sweep-out rate but reduces

the binding energy of the exciton in the well. Hence, this reduces saturation, but thus increases the exciton absorption peak linewidth and so reduces the low intensity electroabsorption effect.

Five wafers were designed to investigate the electroabsorption properties of MQW InGaAsP materials with a range of parameters. In all the structures, the ternary and quaternary materials were lattice matched to InP and an intrinsic region width of 1 $\mu$m was used. The structures are given in Table 1, and the generic p-i-n test diode structure is shown in Fig. 1.

## III. DESCRIPTION OF DESIGNED WAFERS

The first wafer, W-A, contained an active region of 63 InGaAs wells lattice matched to InP barriers. This material has deep wells, and has been found by other groups to have a low saturation intensity, exacerbated

TABLE 1. InGaAsP MQW wafer structures

W-A

| Repeats | Thickness (nm) | Material | Dopant | Type | Conc ($cm^{-3}$) |
|---|---|---|---|---|---|
| 1 | 300 | InP | Zn | p | 2.0E+18 |
| 1 | 200 | InP (p spacer) | | ud | |
| 1 | 31 | InP spacer | | i | |
| 63 | 8 | LM InGaAs | | i | |
| 62 | 7 | InP | | i | |
| 1 | 31 | InP spacer | | i | |
| 1 | 500 | InP | Si | n | 2.0E+18 |

W-B

| Repeats | Thickness (nm) | Material | Dopant | Type | Conc ($cm^{-3}$) |
|---|---|---|---|---|---|
| 1 | 300 | InP | Zn | p | 2.0E+18 |
| 1 | 200 | InP (p spacer) | | ud | |
| 1 | 250 | InP spacer | | i | |
| 1 | 500 | Q1.52 | | i | |
| 1 | 250 | InP spacer | | i | |
| 1 | 500 | InP | Si | n | 2.0E+18 |

W-C

| Repeats | Thickness (nm) | Material | Dopant | Type | Conc ($cm^{-3}$) |
|---|---|---|---|---|---|
| 1 | 300 | InP | Zn | p | 2.0E+18 |
| 1 | 200 | InP (p spacer) | | ud | |
| 1 | 125 | InP spacer | | i | |
| 42 | 12 | Q1.57 QW | | i | |
| 41 | 6 | Q1.15 barrier | | i | |
| 1 | 125 | InP spacer | | i | |
| 1 | 500 | InP | Si | n | 2.0E+18 |

W-D

| Repeats | Thickness (nm) | Material | Dopant | Type | Conc ($cm^{-3}$) |
|---|---|---|---|---|---|
| 1 | 300 | InP | Zn | p | 2.0E+18 |
| 1 | 200 | InP (p spacer) | | ud | |
| 60 | 6.5 | LM InGaAs QW | | i | |
| 61 | 10 | Q1.1 barrier | | i | |
| 1 | 500 | InP | Si | n | 2.0E+18 |

W-E

| Repeats | Thickness (nm) | Material | Dopant | Type | Conc ($cm^{-3}$) |
|---|---|---|---|---|---|
| 1 | 300 | InP | Zn | p | 2.0E+18 |
| 1 | 200 | InP (p spacer) | | ud | |
| 60 | 9 | Q1.6 QW | | i | |
| 61 | 7.5 | Q1.1 barrier | i | | |
| 1 | 500 | InP | Si | n | 2.0E+18 |

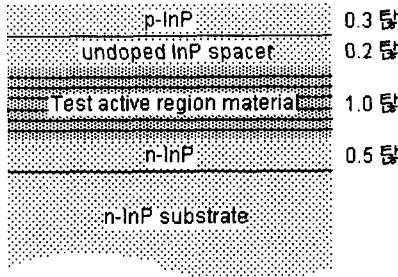


FIG. 1. Generic wafer structure used for investigating active region materials.

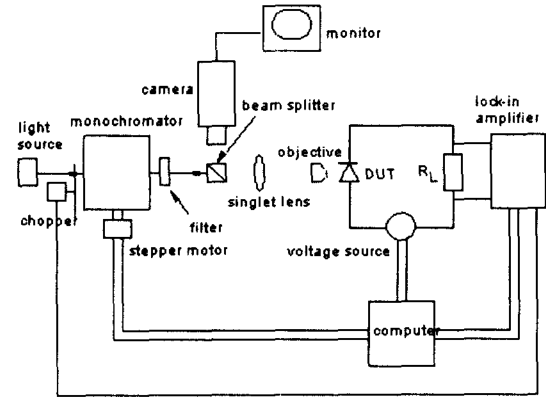


FIG. 2. Monochromator experimental setup for diode photoresponsitivity experiments.

by the large band offset, making $\Delta E_g$ for the holes very large, with consequently long lifetimes. The second wafer, W-B, contained an active region of bulk InGaAsP, intended to investigate the strength of the Franz-Keldysh electro-optic effect in this material. Used in a number of waveguide designs, despite its relatively low electro-optic efficiency, because of its polarisation independent characteristics, this advantage is not applicable for normal cavity devices where the light is always TE. However, its saturation intensity and speed should be better than quantum well materials, and its use simplifies growth. The third wafer, W-C, contained an active region based on that of a high speed, high saturation intensity waveguide modulator developed at France Telecom/CNET [10]. The wafer comprised 42 shallow quaternary wells and quaternary barriers, whose small $\Delta E_g$ should ensure low carrier lifetimes. The final two wafers W-D and W-E, contained wells with $\Delta E_g$ values between those of W-A and W-C. Wells of InGaAs were used in W-D, while the wells of W-E and the barriers of both wafers were of quaternary InGaAsP material. A buffer layer of 200 nm not-intentionally doped material between the p-layer and active region was included to prevent the diffusion of the zinc dopant into the active region. The W-D wafer has 60x65nm InGaAs wells and 61x100nm Q1.1 barriers. The wafer, W-E has 60x90nm Q1.6 InGaAsP wells and 61x75nm Q1.1 barrier. Measurements of the p- and n-doping carried out at University of Sheffield indicated a concentration of around $10^{18}\text{cm}^{-3}$, while the background doping in the i-region was less than $10^{16}$ $\text{cm}^{-3}$.

## IV. PHOTOCURRENT MEASUREMENTS

A method of obtaining the absorption spectra of the material is to carry out photocurrent measurements of the sample. The absorption is related to the photocurrent $i_{ph}$ by

$$i_{ph} = \frac{P\eta(i-R)e}{h\nu}[1-\exp(-\alpha L)] \quad (2)$$

where $P$ is the incident power, $\alpha$ is the absorption coefficient at the photon energy $h\nu$, $L$ is the total thickness of the active region, $R$ is the reflectivity from the surface of the wafer and $\eta$ is the quantum efficiency. Photodiodes were processed from the wafers by etching 200 $\mu$m and 400 $\mu$m diameter mesas through the p- and i-layers and depositing p- and n-contact metals, the p-contacts on the top of the mesas and with a circular shape to allow optical access. The p-contact metal was Au/Zn, the n-contact was Au/Si and both were annealed to reduce the contact resistance. The photoresponsitivity of the diodes were measured at UCL using a monochromator, with the experimental set-up shown in Fig. 2. Noise in the measurements due to external sources was minimised by chopping the incident light and amplifying the photocurrent with a lock-in amplifier.

The photocurrent spectra of wafer W-A with bias voltages 0 - 10 V were measured. No exciton peak was evident and the shift of the absorption edge was very small. One possible explanation for this result is As

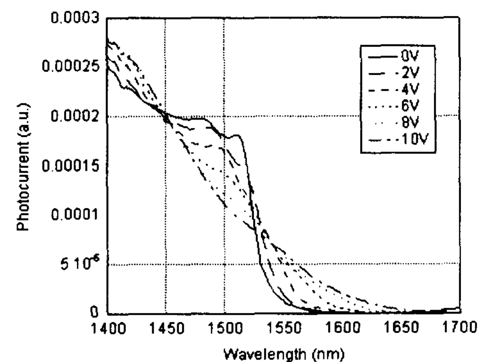


FIG. 3. W-C photocurrent spectra.

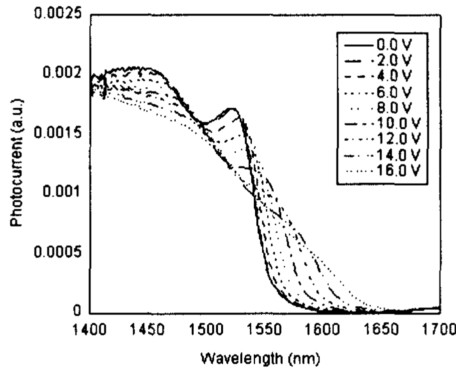


FIG. 4. W-D photocurrent spectra.

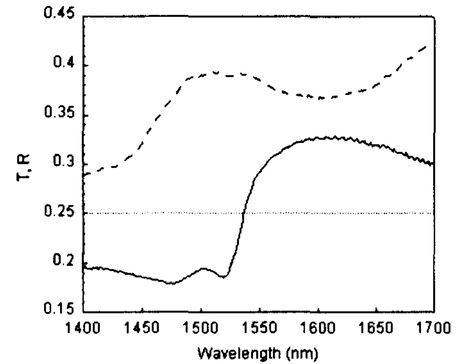


FIG. 6. Measured transmission (solid line) and reflectivity (dashed line) for W-E.

diffusion into the InP barriers during growth, altering the shape of the wells. The photocurrent spectra of W-B exhibited a broadening of the absorption edge in accordance with previously measured Franz-Keldysh effects. The photocurrent spectra of W-C are shown in Fig. 3. An exciton peak can be seen in the 0 V spectrum, evidence of exciton confinement in the wells. Due to the low depth and large width of the wells, increasing the voltage rapidly quenched the exciton, and so little Stark shift of the exciton energy can be seen. The measured photocurrent spectra of W-D, shown in Fig. 4, showed a clear exciton peak and, unlike that of W-E, this was not quenched so rapidly but was red shifted with increasing voltage. A similar effect was seen with W-E (see Fig. 5), although occurring more rapidly at lower voltages.

To convert the photocurrent data to absorption values, Eq. (2) is used, rewritten as

$$i_{ph} = K[1 - \exp(-\alpha L)] \tag{3}$$

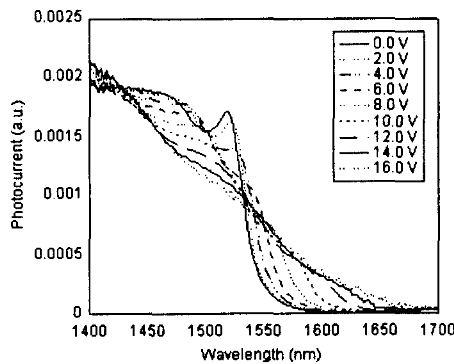


FIG. 5. W-E photocurrent spectra.

To find the scaling factor, the absorption spectrum of the wafer at 0 V is found by measuring the light transmitted through and reflected from an unprocessed piece of the wafer. These measurements for W-E are shown in Fig. 6.

The absorption coefficient is found from the equation

$$\alpha = -\frac{1}{d}\ln\left(\frac{T}{1-R}\right) - C \tag{4}$$

where $C$, an offset due to the absorption in the substrate and other losses, is assumed to be constant over the wavelength range and is found by setting $\alpha$ at lower energies than the bandgap energy to zero. The uniformity of the transmission $T/(1-R)$ through the substrate alone was measured and found to vary by only 6% over the 1500-1600 nm wavelength range of interest. The scaling factor, $K$, in Eq. (3) is found by

$$K = \frac{i_{ph}}{1 - \exp(-\alpha L)} \tag{5}$$

Plots of $i_{ph}$ and $1-\exp(-\alpha d)$ for $E$ and the calculated value of the scaling factor $K$ can be seen in Fig. 7.

Although $K$ is wavelength dependent, due to the factors $P$, $R$ and $h\nu$, it remains fairly constant over the wavelength range of interest. This can be seen from the value of $K$ calculated from the measured spectra in Fig. 7 over the wavelength range 1450 - 1550 nm. At wavelengths longer than this, the low values of absorption mean that small experimental errors in the photocurrent and transmission experiments result in large errors in the calculated value of $K$. Hence, in this case, a value $K = 0.0041$ is used over the whole 1400 - 1700 nm range. A second assumption is that

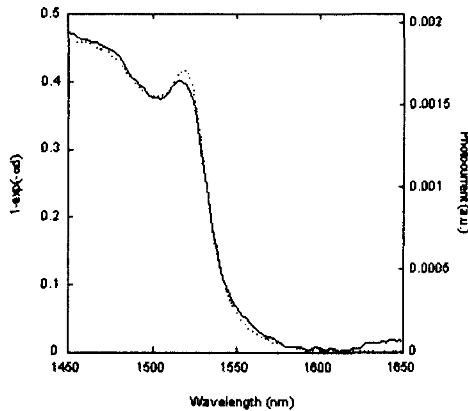


(a)

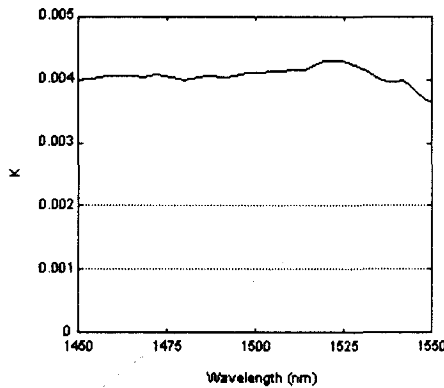


(b)

FIG. 7. (a): A comparison of the photocurrent (solid line) and $1 - \exp(-\alpha d)$, calculated from the results of a transmission/reflection measurement (dashed line), for W-E. (b): Calculated values of $K$.

the quantum efficiency, $\eta$, is independent of applied voltage. This can be assumed, as the photocurrent in the continuum part of the spectrum, at shorter wavelengths than the exciton, remains the same over the voltage range. This indicates that the recombination rate of the photo-generated carriers does not change with applied field, the majority of the carriers are collected in the photocurrent, and hence $\eta$ is close to unity.

Once the value of $K$ has been found, the absorption spectra for the range of voltages can be calculated from the absorption spectra using

$$\alpha = -\frac{1}{d} \ln\left(1 - \frac{i_{ph}}{K}\right) \tag{6}$$

These are shown in Fig. 8 for wafers W-C, W-D and W-E.

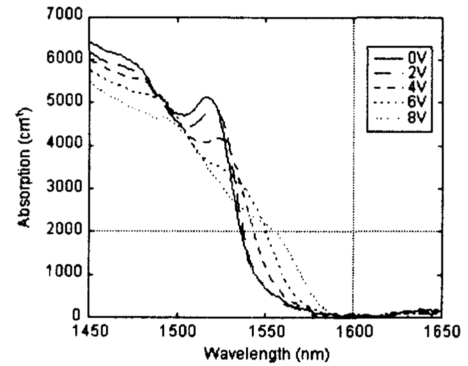


(a)

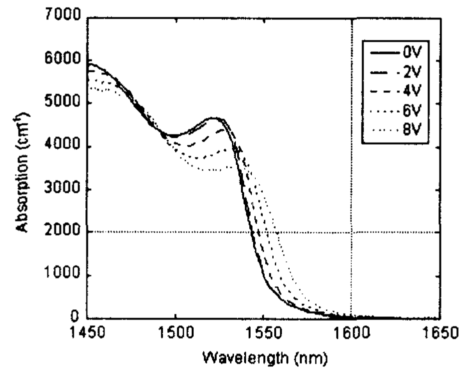


(b)

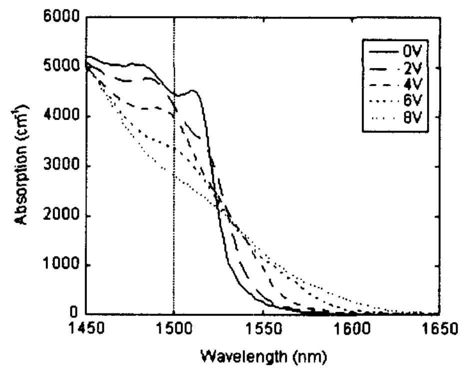


(c)

FIG. 8. Absorption spectra calculated from photoresponsitivity measurements. (a): W-C. (b): W-D. (c): W-E.

The absorption changes of W-D and W-E are greater than those of W-C, explained by the increased exciton confinement in the deeper wells of the first two. A typical operating voltage swing for a microwave

modulator is ~4 V peak-to-peak. If a DC bias of 4 V is applied to a device with a 1 $\mu$m thick i-region, the efficiency of the device would not be impaired by the relatively small absorption change over the range 0 - 2 V. Over the range 2 - 6 V, the absorption increase of W-E is greater than that of W-D and has a lower background absorption, hence making it the most efficient material over this voltage range. At 8 V, the absorption change with voltage drops off and starts to become negative for W-E, while it continues to increase for W-D due to the higher exciton confinement. Hence, W-D would be the more efficient material to use in a modulator working with a higher voltage swing, or a thinner active region.

## V. BIASED TRANSMISSION EXPERIMENTS

Errors in the calculation of absorption spectra from photoresponsivity described in the previous section are introduced due to two reasons: (i) the assumption of a wavelength and voltage independent scaling factor and (ii) the use of different parts of the non-uniform wafer for photoresponsivity and transmission experiments. To obtain a more accurate measurement of the W-E absorption spectra for a range of voltages and to check the accuracy of the spectra found in the previous section, transmission experiments on the wafer with a range of bias voltages were carried out.

The device design was similar to the photodetector described in the previous section. Windows in the n-contact on the back of the substrate allowed the light to pass through the wafer and be detected externally by a separate photodetector, and a quarter-wave thick antireflecting coating of $Si_3N_4$ in the window reduced reflections from this surface. The transmission and reflectivity characteristics of these single pass transmission modulators were measured with a monochromator as before, with the setup shown in Fig. 9.

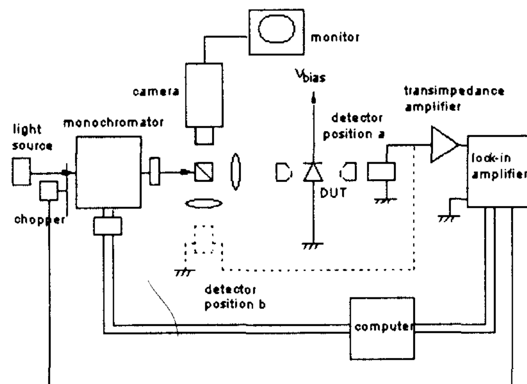


FIG. 9. Monochromator experimental setup for biased transmission and reflection measurements. Detector in position a for transmission, in position b for reflectivity measurements.

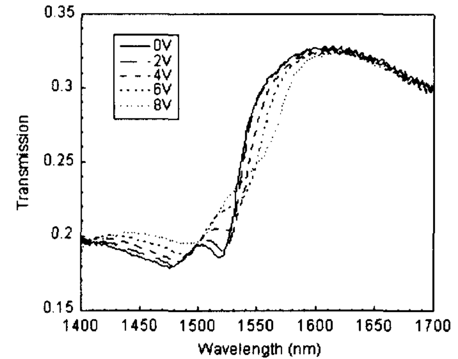


FIG. 10. W-E transmission spectra.

The device transmission spectra are shown for the voltage range 0 - 8 V in Fig. 10. The measured transmission and reflecitivity spectra were used in Eq. (4) to calculate the absorption spectra. The results were very similar to those found from the photoresponsivity experiments, as can be seen in Fig. 11.

## VI. CALCULATING THE REFRACTIVE INDEX CHANGES

The change in the refractive index of the material with bias voltage is an important factor in the calculation of the phase characteristics of a modulator. These changes can be derived from the absorption changes using the Kramers-Kronig. In theory, knowledge of the complete absorption spectrum is required to com-

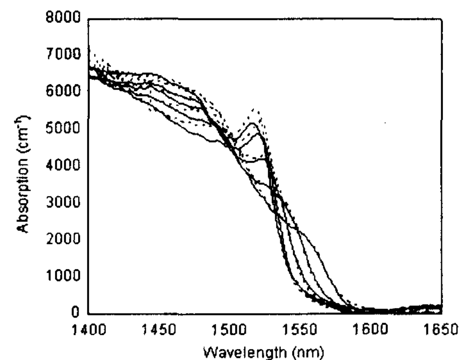


FIG. 11. W-E absorption spectra at 0, 2, 4, 6 and 8 V, calculated from transmission (solid lines) and photoresponsivity (dashed lines) experiments.

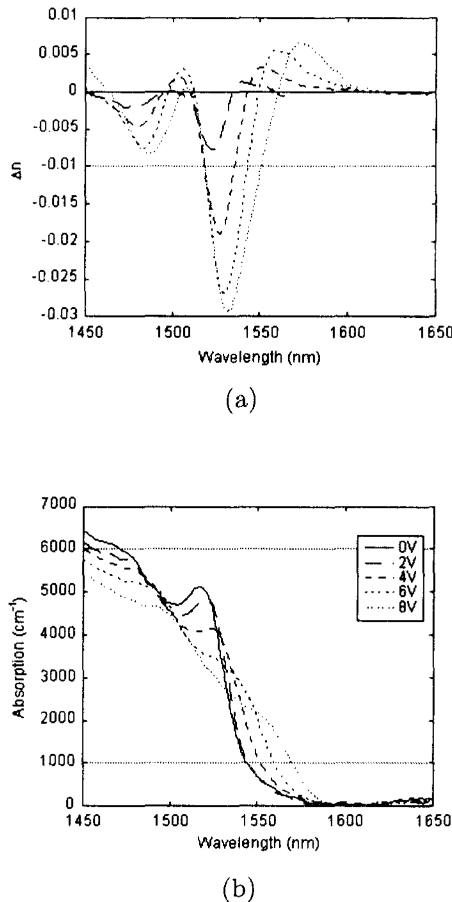


FIG. 12. W-E absorption (a) and refractive index change (b) plots.

pute the real part of the refractive index, or vice versa, since the integral covers the range 0 to $\infty$. In practice, for the MQW structures, we shall only be interested in the possibility of using the changes taking place to produce a modulation, and so we restrict the range of integration to the region of the absorption spectrum close to the fundamental absorption edge, where the notable changes in absorption occur. The change in refractive index, $\Delta n$, caused by an applied voltage, $V$, becomes:

$$\Delta n(\lambda, V) \approx \frac{1}{2\pi^2} \cdot P \cdot \int_{\lambda_1}^{\lambda_2} \frac{\Delta\alpha(\lambda', V)}{1-(\lambda'/\lambda)^2} d\lambda' \qquad (7)$$

where $\lambda_2 > \lambda_1$. $P$ represents the Cauchy principal value of the integral, which means avoiding the critical point $\lambda' = \lambda$ in the integrand by integrating in two parts, from $\lambda_1$ to $\lambda - \delta$, and from $\lambda + \delta$ to $\lambda_2$, with $\delta \rightarrow 0$. $\Delta\alpha$ is the absorption change spectra. Thus, given a reasonably wide range of absorption data for different bias voltages, the corresponding electro-refractive effects can be computed. To get more accurate refractive index change data, wider wavelength range, which is $\lambda_1 \sim \lambda_2$ (1400nm $\sim$ 1800nm), was used in this calculation. The refractive index change results are shown together with the absorption spectra in Fig. 12.

## VII. CONCLUSION

The measurement of absorption coefficient for various QCSE InGaAsP/InP MQW structures was carried out. A range of quantum well designs, ranging from deep InGaAs wells with InP barriers, through to shallower InGaAs and InGaAsP wells with InGaAsP barriers and finally to bulk InGaAsP were investigated. The absorption spectra over a range of applied electric fields were obtained from measured photocurrent spectra. It was expected that the electroabsorption effect would become weaker with the reduction in the depth of the wells, and this was found experimentally, except in the case of the InGaAs/InP MQW structure, which exhibited the lowest electroabsorption effect of all the structures. This could be explained by diffusion of As from the wells into the barriers during growth. The measurement of the transmission of light through biased devices fabricated from W-E confirmed the spectra obtained from the photocurrent measurements. The refractive index changes with applied voltage were calculated from the electroabsorption spectra using the Kramers-Kronig expression.

## ACKNOWLEDGEMENT

This work is mainly supported by Dr. R. Killey, UCL. The authors would like to thank people who are concerned of Imperial College, University of Sheffield, Oxford University and CERN for wafer design, wafer growth and their support.

*Corresponding author : j.song@ee.ucl.ac.uk.

## REFERENCES

[1] U. Koren, T.L. Koch, H. Presting, and B.I. Miller, Appl. Phys. Lett. **1**, 368 (1987).
[2] T. H. Wood, J. Lightwave Technol. **6**, 743 (1988).
[3] J. P. King, I. Hardcastle, H. J. Harvey, P. D. Greene, B. J. Shaw, M. G. Jones, D. J. Forbes, and M. C. Wright, Electron. Lett. **31**, 1090 (1995).
[4] J. B. Song, C. C. Button, and A .J. Seeds, Electron. Lett. **37**, 426 (2001).
[5] D. S. Chemla, T. C. Damen, D. A. B. Miller, A. C. Gossards, and W. Wiegmann, Appl. Phys. Lett **42**, 864 (1983).

[6] A. J. Mosely, D. J. Robbins, A. C. Marshall, M. Q. Kearly, and J. I. Davies, Semicond. Sci. Technol. **4**, 184 (1989).

[7] M. Sugawara, T. Fuji, S. Yanazaki, and K. Nakajima, Phys. Rev. B. **42**, 9587 (1990).

[8] Y. Kutito, N. Yokouchi, T. Miyamoto, F. Koyama, and K. Iga, Jpn. J. Appl. Phys. **34**, 5626 (1995).

[9] A. M. Fox, D. A. B. Miller, G. Livescu, J. E. Cunningham, and W. Y. Jan, J. Quantum Electron. **27**, 2281 (1991).

[10] F. Devaux, F. Dorgeuille, A Ougazzaden, F. Huet, M. Carre, A. Carenco, M. Henry, Y. Sorel, J. F. Kerdiles, and E. Jeanney, IEEE Photon. Technol. Lett. **5**, 1288 (1993).